Lineshapes in core-level photoemission from metals: III. Site-dependent screening in the charge density wave materials 1T- and $4H_b - TaS_2$

1996 J. Phys.: Condens. Matter 8 1457

(http://iopscience.iop.org/0953-8984/8/10/016)

J. Phys.: Condens. Matter **8** (1996) 1457–1473. Printed in the UK

Lineshapes in core-level photoemission from metals: III. Site-dependent screening in the charge density wave materials 1T- and $4H_b$-TaS_2

H P Hughes and J A Scarfe

Cavendish Laboratory, University of Cambridge, Cambridge CB3 0HE, UK

Received 5 October, in final form 18 December 1995

Abstract. High-resolution x-ray photoemission (XPS) studies of the lineshapes of the Ta 4f core levels in 1T- and $4H_b$-TaS_2 are reported. These materials show charge density wave (CDW) behaviour at room temperature, and the local electron densities at different atomic sites are shown to produce different local screening of the core-level photohole, so the components of the doublet or triplet 4f emission line resulting from the CDW-induced shifts in the local potential at different atomic sites have different core line asymmetries. The complex lineshapes are analysed using the iterative fixing procedure, SHAPER, allowing connections to be made between the observed spectra and the site-dependent density of states.

1. Introduction

Paper II [1] was concerned with 2H-TaS_2, a polytype involving only layers of TaS_2 with trigonal prismatic co-ordination of the Ta atoms by the S atoms, and with a unit cell two layers deep. Polytypes also exist in which the hexagonal sheets of Ta and S are stacked within a layer to produce octahedral co-ordination of the Ta by S, and the commonest is the 1T polytype, with a unit cell one layer deep. The overall electronic structure is similar to that for 2H-TaS_2, with the Ta d bands lying above the main bonding S 3p valence bands, and the Fermi energy E_F lying towards the bottom of the Ta d band which holds one electron per formula unit. In detail however, the conduction band structure differs from that for 2H-TaS_2, and the properties associated with the Fermi surface are quite different. In particular, the charge density wave (CDW) behaviour is markedly different, and a strong periodic lattice distortion (PLD) exists for 1T-TaS_2 even at room temperature. A further polytype of interest is $4H_b$-TaS_2, in which alternate layers of trigonal prismatic (2H-like) and octahedral (1T-like) layers are stacked with a four-layer repeat. Because of the relatively weak interlayer interaction in these materials, $4H_b$-TaS_2 simultaneously shows properties which reflect both types of layer rather than some averaged behaviour. Following a preliminary report [2], a full analysis of the XPS data for 1T and $4H_b$ materials is presented here in two sections, with the discussion for 1T-TaS_2 leading naturally to that for $4H_b$-TaS_2.

The CDW has dramatic effects upon the Ta 4f XPS emission: the different sites within the enlarged in-plane unit cell have different local electron densities and therefore different chemical shifts, so each 4f line for 1T-TaS_2 is split into a clear doublet [3, 4], and for $4H_b$-TaS_2 a striking triplet structure is observed as will be shown below. But the CDW has effects beyond these straightforward splittings, and it will be shown that the different local charge densities and the related joint densities of states at the various Ta sites give rise to

0953-8984/96/101457+17$19.50

different screening of the core-level photohole, manifested by the different asymmetries of the multiplet lines arising from the different sites. These lineshape parameters are extracted from the experimental data presented here (obtained at high resolution using synchrotron radiation at the UK EPSRC Daresbury Laboratory) using the analysis package SHAPER, described in paper I [5], which sets out the underlying theory and details of the computational approach and implementation. Experimental details are straightforward and have been given earlier [1].

2. 1T-TaS_2

2.1. Conduction band structure

1T-TaS_2 has a complex phase diagram: Wilson *et al* [6, 7] first observed a PLD in 1T-TaS_2 associated with a CDW in which the electron density at each atomic site in a crystal layer is modulated by a two-dimensional wave spanning several unit cells. Below 180 K the PLD–CDW combination forms a stable ground state, the $1T_3$ phase, in which the CDW–PLD forms an in-plane $\sqrt{13} \times \sqrt{13}$ superlattice commensurate with the underlying lattice. Above 180 K the $1T_2$ phase is 'quasi-commensurate' [8], and above 352 K the $1T_1$ phase is fully incommensurate. The commensurate $\sqrt{13} \times \sqrt{13}$ $1T_3$ phase, which is concentrated upon here and will be used as a basis for discussion for the room-temperature data, has a unit cell of 13 Ta atoms and three geometrically distinct Ta sites [9] (a, b, c, with one atom at site a, six at site b, and six at site c) which form a star-shaped array in the sheet of Ta atoms (figure 1). The different CDW-induced charge densities at these sites give rise to chemical shifts in the binding energy of the core levels and the well known splitting of the Ta 4f core-level XPS line [4, 10, 11]. It will be shown that the CDW-induced modifications of the conduction band structure [12] also result in different screening of the core photoholes at different sites, so that the components of the split 4f line have different lineshapes. The phase and amplitude of the CDW are not clear from first principles. Early empirical chemical shift arguments [3] suggested a large amplitude of ~ 1 electron and another estimate [13] based on chemical shifts and a self-consistent calculation suggested 0.05 electrons. Scanning tunnelling microscopy (STM) measurements [14] and more recent models [12] suggest an amplitude of a considerable fraction of an electron—an electron excess (on sites a and b) and a deficit (on site c) of the order of 0.4 electrons—and a corresponding significant modulation of the local density of states (LDOS) at each site.

A full band structure calculation for $1T_3$-TaS_2 would be difficult (the unit cell includes 39 atoms), but Smith *et al* [12] have developed a simple model (figure 2) for the narrow Ta d-like conduction bands based on the LCAO method which, though it does not match the angle-resolved photoemission (and inverse photoemission) data [9, 12, 15] in every detail, is a useful starting point for the analysis of the core-level photoemission lineshapes. The ordinarily fairly simple Ta d-band manifold [12, 16] is split into three by the CDW. The LDOS at E_F ($= 0$) is different for each site, being high for site a, and lowest for site b, and the number of d electrons at each site (i.e. the integrated LDOS up to E_F) are calculated to be 1.455, 1.311 and 0.611 for sites a, b and c respectively; the mean occupancy, weighting appropriately in the ratio 1:6:6, is unity. The different total occupancies account for the splitting [4, 11, 13] of the Ta 4f core-level lines, with photoelectrons from Ta core levels at site c appearing at lowest KE (highest binding energy), photoelectrons from b at higher KE and a slightly higher still; the total emission intensity from sites a:b:c should clearly be in the ratio 1:6:6.

The different LDOS, particularly close to E_F, should also give different lineshapes,

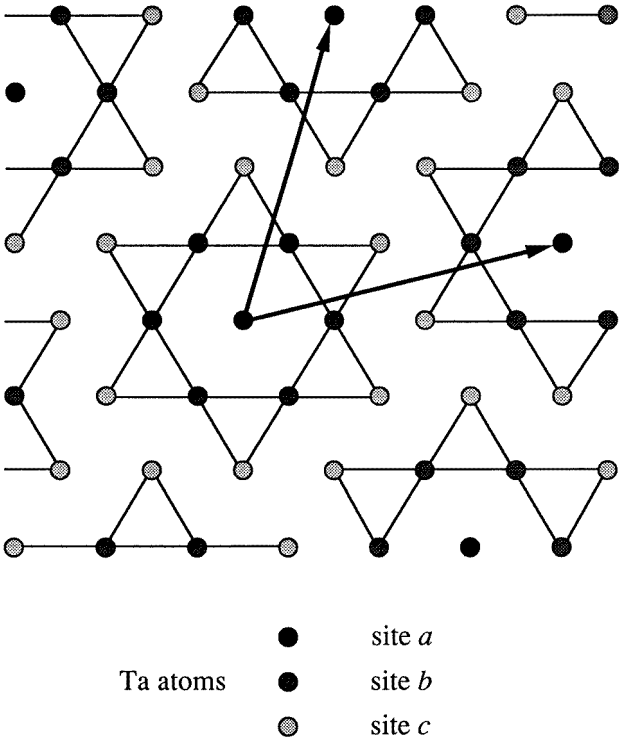

Figure 1. A schematic diagram of the $\sqrt{13} \times \sqrt{13}$ superlattice in 1T-TaS_2; the circles represent Ta atoms in the central sheet of the 1T layer, and the shadings distinguish the inequivalent Ta sites resulting from the CDW. The arrows indicate the superlattice basis vectors.

since the density of excitations ($J(E)$) in the conduction band determines the shape of the asymmetric tail. $J(E)$ is approximated by the joint density of states (JDOS) expected for each type of site, calculated (figure 3) by convolving the empty and occupied states from the model LDOS of Smith *et al* [12]. Unfortunately, the model LDOS extends only to 0.4 eV above E_F, and a $J(E)$ up to 0.4 eV is inadequate to describe the full core-level lineshape, particularly because $J(E)$ is still rising near 0.4 eV; the details of $J(E)$ over such a narrow energy range will also not be observable in a core-level line with a width of similar magnitude. However, the initial slope of $J(E)$, which determines the asymmetry of the XPS line close to its peak (paper I), will be considerably higher for emission from site a compared with b and c, and a smaller difference in asymmetry between sites b and c is also expected.

The model on which these predictions are based is simplistic, and the energy scale for the LDOS was adjusted [12] to fit angle-resolved photoemission data, but gives an excellent starting point for analysing the relationship between the core-level lineshapes and the conduction band structure.

2.2. XPS data on 1T-TaS_2

Figure 4 shows one of five XPS spectra, analysed using SHAPER, for the Ta 4f core level of 1T-TaS_2 measured at 160 K. The energy resolution is better than for earlier work [4, 11]

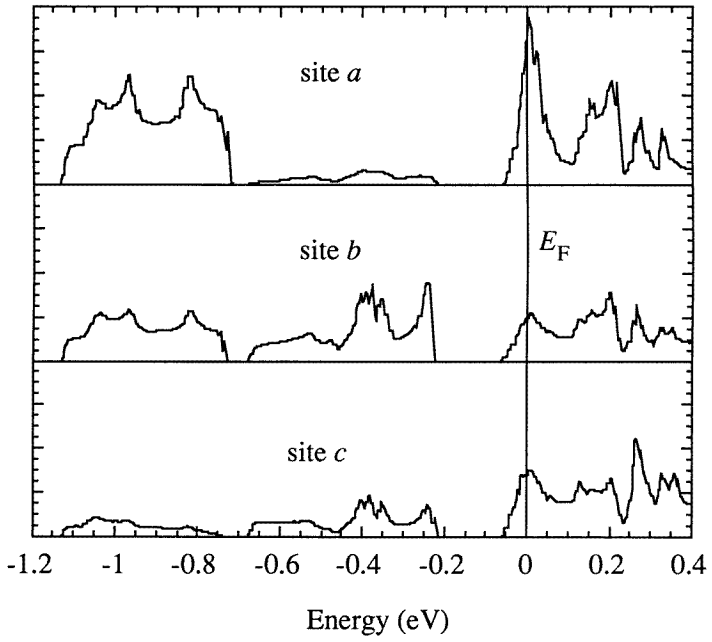

Figure 2. Model LDOSs (in arbitrary units) on each of the three sites in 1T-TaS_2 from Smith *et al* [12]. E_F is at zero on the horizontal axis.

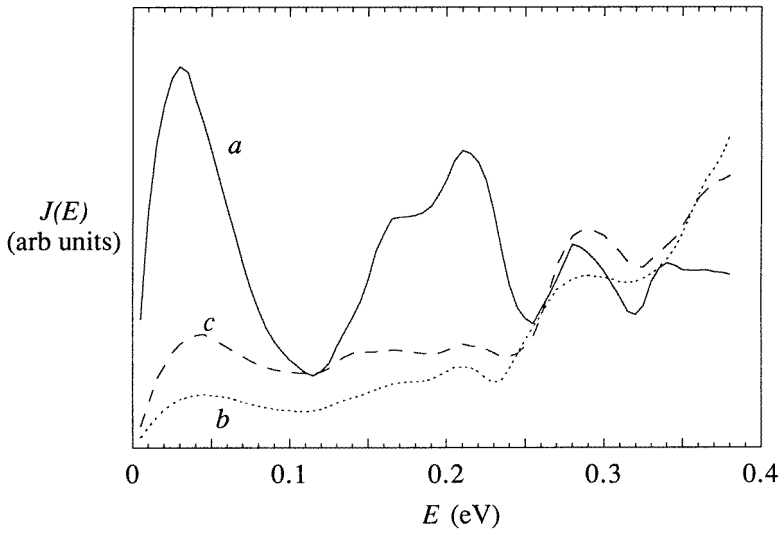

Figure 3. The joint densities of states $J(E)$ at sites a (——), b (· · · · · ·) and c (– – –) in 1T_3-TaS_2 derived from the densities of states of Smith *et al* [12]. No matrix element is included in the calculation.

because of the superior resolution of the incident 80 eV synchrotron radiation. The overall structure shows the spin–orbit doublet (with the Ta final state either $J = \frac{5}{2}$ or $J = \frac{7}{2}$ with

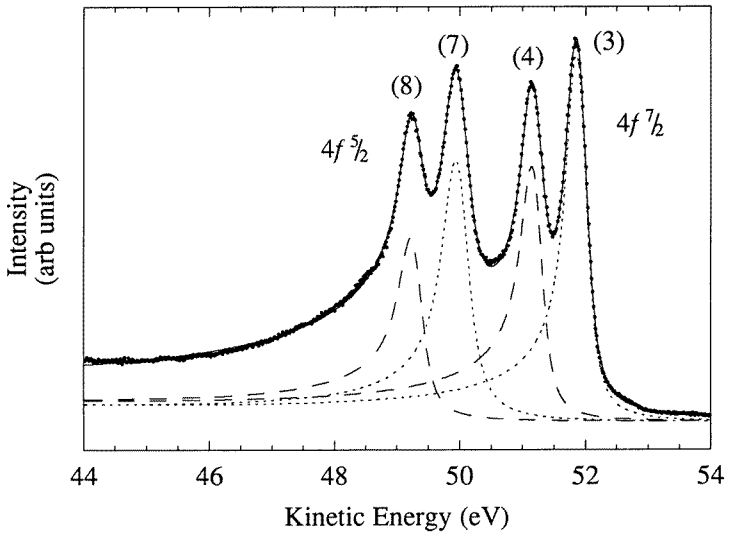

Figure 4. Four-peak fits to the Ta 4f levels in photoemission from $1T_3$-TaS_2 using 80 eV photons and the simple DS lineshape. In this and later figures, each fitted component is shown superposed on the fitted background for display purposes, so the sum of the components does not match the total fit.

the expected 8:6 ratio of emission intensities, and each component of the spin–orbit doublet is further divided by CDW-induced core-level shifts as described above; the higher the conduction electron density at a Ta site, the higher the (mean) KE of the 4f photoelectrons. Two peaks are obvious, but the discussion above suggests that there should be a third—a CDW-split *triplet* in the ratio 1:6:6; however, the heights of the component peaks are apparently different, so the weakest line might be coincident with one of the others. Note also that the widths of the peaks for $J = \frac{5}{2}$ seem greater than those for $J = \frac{7}{2}$. The sharpness of the peaks makes it straightforward to obtain approximate values for the spin–orbit splitting ΔE_{SO} ($= 1.9 \pm 0.1$ eV), and that due to the CDW ΔE_{CDW} ($= 0.7 \pm 0.1$ eV).

Spectra at photon energies of 70 eV (not shown) are very similar, apart from the obvious difference in the KE at which the peaks are centred, and narrower linewidths at 70 eV due to improved resolution. However, a weak shoulder is much more apparent in the 80 eV spectrum in figure 4 at about 52.5 eV than in the 70 eV spectrum (where it is expected at 42.5 eV); this is not a constant-KE feature (e.g. an Auger peak), and is discussed in more detail later. It is difficult to assess by eye any differences in asymmetries of individual peaks arising from electron–hole pair formation in the conduction band (paper I), and these details will be examined below using SHAPER.

2.3. Fits to 1T-TaS_2 XPS data using SHAPER

Five Ta 4f spectra were analysed using SHAPER, two obtained with a photon energy of 80 eV, three with 70 eV, and representative fits are presented in this section. The datasets each contain 624 data points, so the value of the goodness-of-fit parameter ρ obtained (see paper I) should be distributed as $\chi^2_{624-\mu}$ where μ is the number of free fitting parameters. As usual, it is difficult to assess the noise distribution accurately, so 624–μ is not strictly appropriate, but a 'perfect' fit should have ρ close to 600.

First the spectra were fitted using with four DS lines (i.e. using JDOS-A of figure 4 in paper II). The Gaussian widths from the instrumental resolution were constrained to be the same for all peaks, but the Lorentzian lifetime widths were unconstrained. The amplitudes (total integrated area) of the CDW-split peaks in each doublet were constrained to be equal. The fitting results are shown with the data in figure 4. (The component peaks are numbered in descending order of kinetic energy and the enumeration allows for further components to be introduced later.) At first sight the fits appear to be fairly good, but the signal-to-noise ratio of these data is good, and, for the fit to be good in statistical terms, the deviations between the data and the fit should be much lower; $\rho = 2261$, more than three times what is required for a 'perfect' fit. Figure 5(*a*) shows the normalized residuals, $Q(E)$, with clear systematic deviations in (i) the tail between 44 and 48 eV, (ii) the immediate vicinity of each peak, (iii) the region between the doublets and (iv) the high-KE end, where a shoulder occurs in the highest-KE peak. (This apparently artificial division of the spectrum is useful for comparison with subsequent fits.) The most significant feature of this fit, which will recur repeatedly below, is the difference in asymmetry (i.e. the slope of $J(E)$) between the peaks, particularly the low asymmetry of peaks 3 and 7 compared with the high asymmetry of peaks 4 and 8: $\alpha_3 = 0.211$; $\alpha_4 = 0.294$; $\alpha_7 = 0.192$; $\alpha_8 = 0.311$. The residuals for the unshown 70 eV spectrum are similar; peaks 4 and 8 are again more asymmetric than peaks 3 and 7.

A further fit was attempted using a refined $J(E)$, linear in E at the origin with slope α, with a freely varying cut-off energy (JDOS-B, see paper I) representing a truncated, flat conduction band, constrained to be the same for peaks 3 and 7, and the same for peaks 4 and 8. The sharpness of the cut-off is constrained to be equal for all peaks, but its position is not; in fact the truncation of $J(E)$ produced by SHAPER for all four peaks occurs at a remarkably consistent energy of 3.90 ± 0.15 eV. The asymmetries of peaks 4 and 8 are again found to be higher than those of 3 and 7: $\alpha_3 = 0.190$; $\alpha_4 = 0.320$; $\alpha_7 = 0.138$; $\alpha_8 = 0.277$. The residuals $Q(E)$ (figure 5(*b*)) show that the fit in the region of the tail (comment (i) above) is very much improved by the change of lineshape model, but most of the other problems ((ii)–(iv)) remain. The ρ-value of 1501.1, representing a modest improvement in the quality of the fit, though reduced, is still far too high for a statistically acceptable fit and it is clearly necessary to refine the lineshape model further.

So far the analysis has been empirical and the four peaks in the spectrum fitted with four lines, but the theoretical structure of the CDW includes *three* distinct Ta sites with total occupations of the conduction band for Ta sites a, b and c of 1.455, 1.311 and 0.611 electrons respectively. The peaks corresponding to sites a and b may be almost superposed and unresolved, but the LDOS of sites a and b are very different, so it is not appropriate simply to increase the amplitude of the higher-KE peak from a ratio of 1:1 to 7:6. A new peak must be introduced with one-sixth of the amplitude of the other two in each part of the doublet, at slightly above the KE of the higher of the two existing peaks, making a total of six lines for the Ta 4f levels. The residuals resulting from such a six-line fit are shown in figure 5(*c*), and superficially resemble those for the previous fit, since the extra two peaks have small amplitude and are so asymmetric that their weight is distributed over a wide energy range, but the fit is markedly improved: the extra peaks have almost entirely removed the discrepancy in the region between the doublets, and fit the shoulder (peak 2) on the high-KE side of peak 3. Only a small (400 counts in 30 000) deviation is observable in the residuals $Q(E)$, and ρ is down to 829; given the uncertain estimate of the errors in the data, this represents a good fit.

The lifetime width of the extra peak in each triplet is not consistently determined, but this is not too surprising as these are less than the Gaussian width of the instrumental

broadening, so the overall lineshapes are not very sensitive to the lifetime width parameters. The energy separation between peaks 2 and 3 (or 6 and 7) is about 0.60 eV. The asymmetry of peaks 2 and 6 is much higher than that of the other four lines, with lines 4 and 8 again significantly more asymmetric than 3 and 7: $\alpha_2 = 0.689$; $\alpha_3 = 0.225$; $\alpha_4 = 0.266$; $\alpha_6 = 0.687$; $\alpha_7 = 0.238$; $\alpha_8 = 0.340$. The similarity in α between corresponding peaks in each triplet suggests that a further constraint—$\alpha_2 = \alpha_6$, $\alpha_3 = \alpha_7$, $\alpha_4 = \alpha_8$— might be appropriate, but $J(E)$ used in the generation of the lineshape is a product of the JDOS with the matrix element for the excitation, and this matrix element may be different for the $J = \frac{7}{2}$ and $J = \frac{5}{2}$ triplets. The best constraint would therefore be $\alpha_2/\alpha_6 = \alpha_3/\alpha_7 = \alpha_4/\alpha_8$, but this would involve the quotients of fitting parameters, a non-linear constraint difficult to incorporate in the fitting process. A computationally simpler option sets this ratio to unity; the resulting distortion must be weighted against the apparent inconsistency if the constraint is omitted.

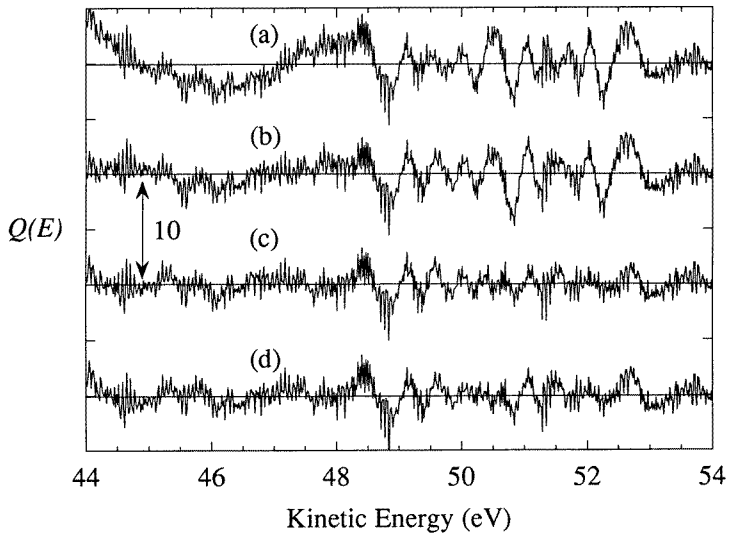

Figure 5. The normalized residuals $Q(E)$ for fits to the Ta 4f levels in $1T_3$-TaS_2 (*a*) for the four-peak fit shown in figure 4, (*b*) for a four-peak fit with linear $J(E)$s with freely varying cut-off energies, (*c*) as for (*b*) but with an extra peak to the high-KE side of each doublet and (*d*) for the six-peak fits shown in figure 6.

The final fit (figure 6) implements this, and the corresponding residuals are shown in figure 5(*d*); the results, including the ρ-value, are not substantially different from the unconstrained six-peak fit, and the relevant parameters are summarized in table 1; the Gaussian width for each peak is 0.293 eV. The trend in the initial slope of $J(E)$, determined by α, remains the same—the difference in α between the lines within each triplet is marked and significant. For the different Ta sites within $1T_3$-TaS_2 there are *different* core-level photoelectron lineshapes, caused by *different* local densities of states in the conduction band. Figure 7 shows the $J(E)$s calculated from SHAPER's output parameters for this fit for the 80 eV spectrum. The variations between the Lorentzian widths and the cut-off energies for the peaks illustrates the difficulty SHAPER has in extracting parameters to which the fit is relatively insensitive; this is particularly marked for the weakest site a peak, for which even the asymmetry appears unphysically large; there are also inevitably some

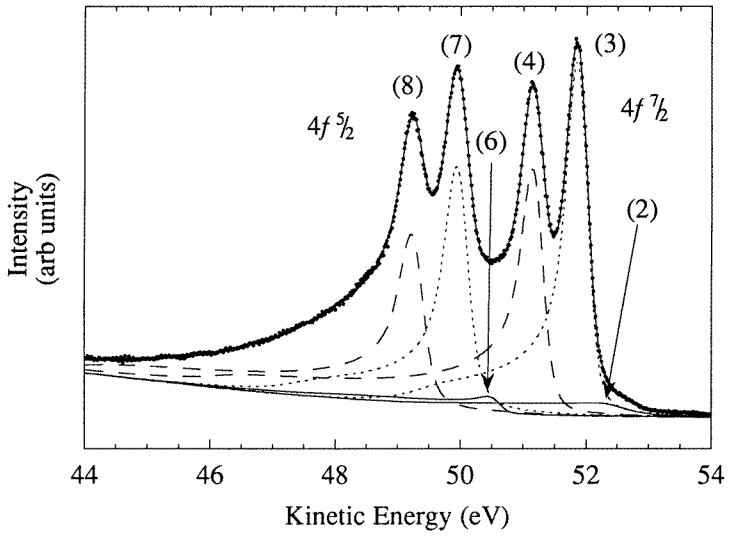

Figure 6. Six-peak fits to the Ta 4f levels in $1T_3$-TaS_2 using a cut-off $J(E)$ with the set of asymmetries (α) within each triplet constrained to be the same for both triplets (i.e. $\alpha_2 = \alpha_5$; $\alpha_3 = \alpha_7$; $\alpha_4 = \alpha_8$).

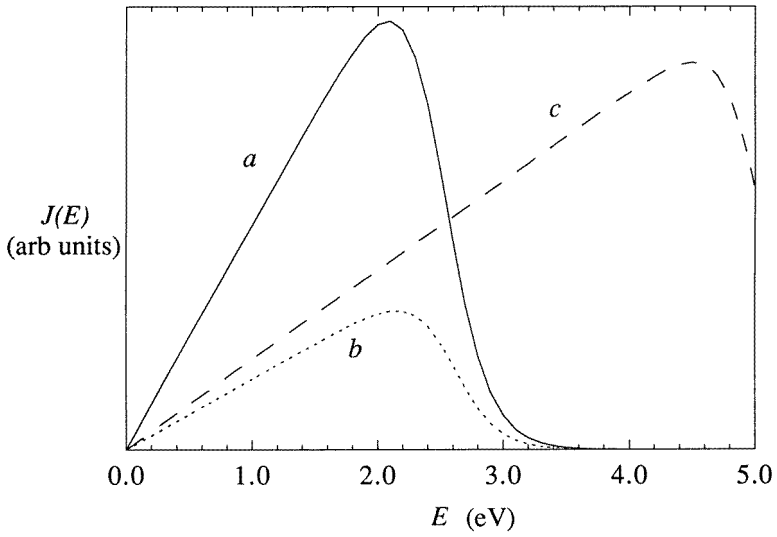

Figure 7. The JDOSs corresponding to the parameters derived from the fits of figure 6.

minor differences between these fits and those to the unshown 70 eV spectra because of the complexity of the fit, but the fit is sensitive to the asymmetry for the stronger peaks, and the trend (that lines 4 and 8 are more asymmetric than 3 and 7) is again clear and reliable.

Table 1. A summary of results of lineshape fits for $1T_3$-TaS_2, $4H_b$-TaS_2 and 2H-TaS_2 (from paper II). Fixed parameters are italicized; those on their upper or lower bounds are indicated by an asterisk. The lines are labelled from high KE (1) to low KE (8).

		$4H_b$-TaS_2	$1T_3$-TaS_2	2H-TaS_2
Photon energy (eV)		70	80	80
Peak kinetic energy (eV)	(1) 2H	42.04		52.07
	(2) 1T site a	42.00	52.48	
	(3) 1T site b	41.58	51.89	
	(4) 1T site c	41.00	51.19	
	(5) 2H	40.14		50.18
	(6) 1T site a	40.10	50.57	
	(7) 1T site b	39.68	49.98	
	(8) 1T site c	39.10	49.27	
Lorentzian widths (eV)	(1) 2H	0.019		0.036
	(2) 1T site a	*0.500*	0.521	
	(3) 1T site b	0.254	0.127	
	(4) 1T site c	0.123	0.123	
	(5) 2H	0.010*		0.001*
	(6) 1T site a	*0.500*	0.010*	
	(7) 1T site b	0.313	0.192	
	(8) 1T site c	0.181	0.179	
Asymmetry (α)	(1) 2H	0.130		0.139
	(2) 1T site a	*0.750*	0.758	
	(2) 1T site b	0.175	0.236	
	(4) 1T site c	0.299	0.303	
	(5) 2H	0.130		0.146
	(6) 1T site a	*0.750*	0.758	
	(7) 1T site b	0.175	0.236	
	(8) 1T site c	0.299	0.303	
Cut-off in $J(E)$ (eV)	(1) 2H	4.44		3.86
	(2) 1T site a	4.12	2.50	
	(3) 1T site b	4.05	2.57	
	(4) 1T site c	9.00	5.06	
	(5) 2H	4.44		3.86
	(6) 1T site a	4.12	2.50	
	(7) 1T site b	4.05	2.57	
	(8) 1T site c	9.00	5.06	
ΔE_{CDW} (eV)		0.58 ± 0.01	0.70 ± 0.01	
ΔE_{SO} (eV)		1.90	1.92	1.90
Amplitude ratio	(1)/(5)	1.759	—	1.600
Amplitude ratio	$\frac{((2)+(3)+(4))}{((6)+(7)+(8))}$	1.420	1.270	—
ρ		516	916	854
Ideal ρ value		297	600	685

2.4. Comments on the electronic structure of 1T-TaS_2

XPS has provided information on the *local* density of states for $1T_3$-TaS_2 where the CDW induces a difference between Ta sites. These conclusions can be compared with the model

of Smith *et al* [12] shown in figure 3. The similarity between the trend in their calculated JDOS and the $J(E)$ from figure 7 is startling. Site a, the minority site, is expected to have by far the greatest JDOS, with site c, despite its lowest overall conduction band occupation, having a higher JDOS than site b. The model of Smith *et al* is simplistic and extends over rather a narrow energy range, but the trend in local densities (and joint densities) of states suggests exactly the ordering of asymmetries found in subsection 2.3.

STM is an excellent probe of local electronic structure and studies of 1T-TaS_2 have been widespread. Most work [8, 14, 17–20] has been on the quasi-commensurate $1T_2$ phase, but STM studies of $1T_3$-TaS_2 and 1T-$TaS_{2-x}Se_x$ complement the XPS results presented here [21–23]. STM images show a large modulation at the CDW wavelength and clusters corresponding to the $\sqrt{13} \times \sqrt{13}$ superlattice centres, and pick out the atomic modulation of the S atoms, so the Ta atom at the centre of the supercell (site a) is marked by the three S atoms above. The z-deflection (closely related to LDOS) plotted in a line across the crystal shows a sharp peak at the centre of the supercell, with a weak atomic-scale modulation superimposed on the baseline. This indicates that the LDOS at E_F is much greater at site a than at the other Ta sites, matching the deduction from XPS that the JDOS is very much more for Ta site a than for the other sites. STM is however unable to register the relative LDOS of sites b and c.

The differences in asymmetry of Ta 4f core-level lines between Ta 4f sites can therefore be attributed to the difference in LDOS at E_F at these distinct sites, an interpretation which concurs well with theoretical predictions and other experimental evidence from STM.

3. $4H_b$-TaS_2

$4H_b$-TaS_2 to an extent combines the properties of 1T-TaS_2 and 2H-TaS_2, but also has some interesting features of its own. The unit cell spans four layers, two with octagonal co-ordination ('1T-like' layers) and two with trigonal prismatic co-ordination ('2H-like' layers) and unsurprisingly its properties reflect the properties of each [24]. Below 22 K it exhibits a 3×3 CDW–PLD characteristic of the 2H polytype, and between 22 and 315 K a $\sqrt{13} \times \sqrt{13}$ CDW–PLD as in the 1T polytype [7, 25]. The XPS measurements described here were carried out at room temperature, on the $\sqrt{13} \times \sqrt{13}$ phase, and can thus be compared directly with the data on 1T-TaS_2 described in the previous section.

However, the reported PLD wavevectors differ slightly from those for 1T-TaS_2 and 2H-TaS_2. Together with shifts in optical data and different lattice parameters, this implies that charge transfer occurs from the octahedral (1T) to the trigonal prismatic (2H) layers [26]. This is likely to have significant effects on the 4f XPS spectra, with the peaks from the trigonal prismatic layer shifted to higher KE than those from the octadhedral layer. More significant, a transfer of charge between layers will change the JDOS, and hence affect the core-level lineshapes for each type of layer. The sharply peaked conduction band DOS in 2H-TaS_2 will accentuate any shift of the conduction band relative to E_F.

3.1. Electronic structure

There are no calculations of the band structure for $4H_b$-TaS_2 to match those for 1T-TaS_2 and 2H-TaS_2. A spin–orbit-split doublet is expected from each type of layer, but, in the case of the octahedral layers, this will be further split by the CDW as for 1T-TaS_2 itself. The immediate consequence of charge transfer between the octahedral and trigonal prismatic layers for the 4f XPS spectrum is that the core-level lines from the trigonal prismatic layers will appear at higher KE than those from the octahedral layers—a straightforward chemical

shift. But the effect on the conduction band JDOS, and hence the asymmetries, is less obvious. If the charge transfer occurs without modifying the shape of the conduction band, the rigid-band model could be applied. In the 2H-like layers, this would cause a shift of E_F relative to the peak of the d_{z^2} band, reducing the density of states at E_F. This, in turn, would reduce the initial slope of $J(E)$ and so decrease the apparent asymmetry of the lines. The effect on the 1T-like layers is unclear, because of the modification of the conduction band by the CDW.

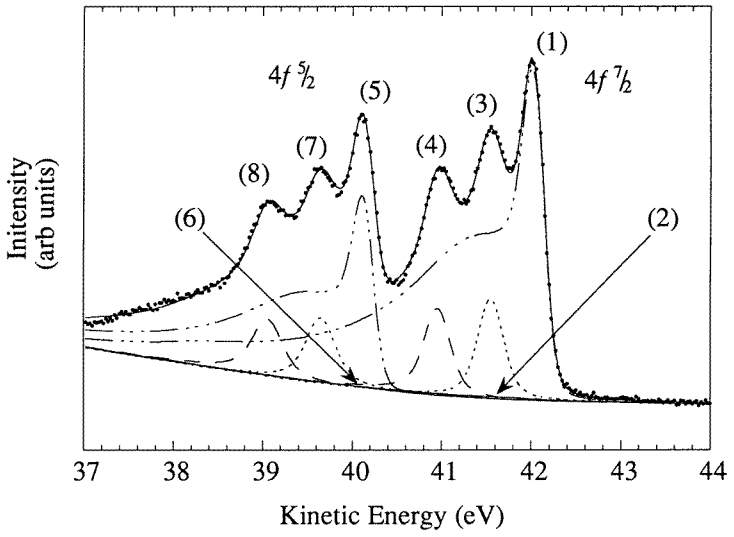

Figure 8. Eight-peak fits to the Ta 4f levels in $4H_b$-TaS_2. All lineshape parameters except α are fixed.

3.2. XPS data

Figure 8 shows a representative XPS spectrum, for an incident photon energy of 70 eV, obtained at room temperature from $4H_b$-TaS_2: the spectrum shows six well resolved peaks which can be assigned as follows. The largest splitting observed is the usual spin–orbit splitting of about 2 eV. This divides the spectrum into two triplets (above and below 40.5 eV); the higher-KE triplet is emission leaving a $J = \frac{7}{2}$ final state, the lower-KE triplet a $J = \frac{5}{2}$ final state; the theoretical intensity ratio is 8:6. The highest-KE peak of each triplet (1 and 5) comes from the 2H-like layer (the '2H line'), with the lowest two (3 and 4, and 7 and 8—the '1T lines') arising from the 1T-like layer, split by the CDW-induced chemical shift as it was in 1T-TaS_2.

Other spectra from different parts of the sample (e.g. figure 9) have less intensity in peaks 1 and 5, confirming the assignment of these peaks to the 2H layer: as the photon beam falls on different areas of the crystal where photoemission is predominantly from one type of layer or the other, it measures different ratios of 2H to 1T emission. The ratio of heights of the lower-KE pair in each triplet is always similar, indicating mixing of sites on an atomic rather than macroscopic scale, and therefore within an octahedral layer. The sharp kink in the spectrum at about 38.5 eV is reminiscent of the shoulder in the 2H-TaS_2 data (paper II). The separation of the 2H line from the 1T line is similar to the splitting of

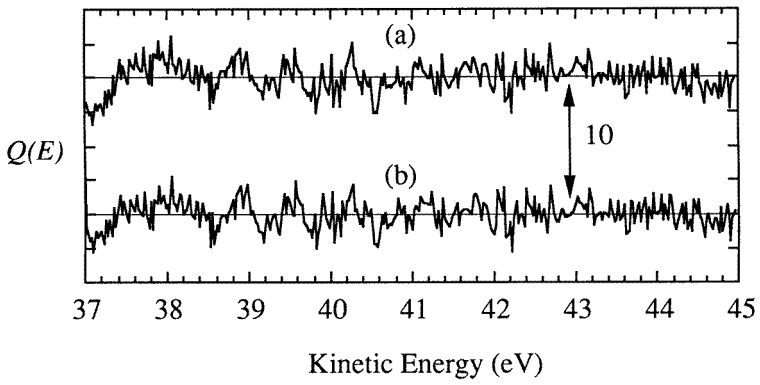

Figure 9. A further spectrum for the Ta 4f levels in $4H_b$-TaS_2, showing a change in the relative intensities of the 1T and 2H lines.

the 1T lines themselves, pointing to an interlayer charge transfer of a similar magnitude to the amplitude of the CDW.

Preliminary estimates of the splittings are $\Delta E_{SO} = 1.9 \pm 0.1$ eV, the same as for 1T-TaS_2, and $\Delta E_{CDW} = 0.6 \pm 0.1$ eV, possibly less than for 1T-TaS_2 (0.7 ± 0.1 eV). Note that the presence of the 2H peak tends to shift the top of the higher-energy 1T peak to higher KE by adding a sloping background, *increasing* the splitting; a *decrease* is indicative of a CDW in the octahedral layers in $4H_b$-TaS_2 that is of lower amplitude than that in 1T-TaS_2. ΔE_{2H-1T}, the difference in binding energy between the 2H peak and the mean of the 1T peaks, is 0.7 ± 0.1 eV; its similarity to ΔE_{CDW} suggests that the magnitude of the charge transfer from octahedral to trigonal prismatic layers is similar to the amplitude of the CDW, that is, a significant fraction of an electron per atom. The 1T peaks are noticeably broader than the 2H peak, but any assignment of asymmetries will require analysis in detail using SHAPER.

3.3. Fits to $4H_b$-TaS_2 XPS data using SHAPER

The analysis is difficult because of the number of lines involved, two from the trigonal prismatic '2H' layer, and six from the octahedral '1T' layer. Further, the mean energy of the lowest-amplitude peak from the 1T layers (from site a), if it occurs at the same relative energy as for 1T-TaS_2, will be almost coincident with the mean energy of the peak assigned to emission from the 2H-like layers. The signal-to-noise ratio of the data is critical in determining whether it is possible accurately to fit lineshapes to a peak incorporating two such closely spaced lines, and a large difference in the amplitudes of the lines makes matters worse. In this case the data are not good enough for such a separation, but the 8% of the emission from sites a in the 1T layers cannot be ignored; the lineshape, and even the width, of the site a peak have consequently been fixed in advance using parameters from the fits on 1T-TaS_2 for the corresponding line, in the expectation that any error associated with this will not significantly disturb the fit to the coincident 2H line.

Fits with simple DS lineshapes have already been shown to be inappropriate for these materials, and it is natural to start from the lineshapes from the best earlier fits. For the IT layers, this was a 'cut-off' $J(E)$, linear in E at the origin with slope α, with a smooth cut-off at an energy given by a separate parameter. In the '2H' layers $J(E)$ had an additional Gaussian subpeak added to it, with height, width and mean energy given by

further parameters (JDOS-D; see paper II). These were used as a starting set for the $J(E)$ parameters, allowing, first of all, only α to differ between the 1T/2H and $4H_b$ fits. The amplitudes, positions and widths of the peaks were allowed to vary, except in the case of peaks 2 and 6, the line from emission from site a from the 1T layer, where the lifetime (Lorentzian) width was fixed as described above.

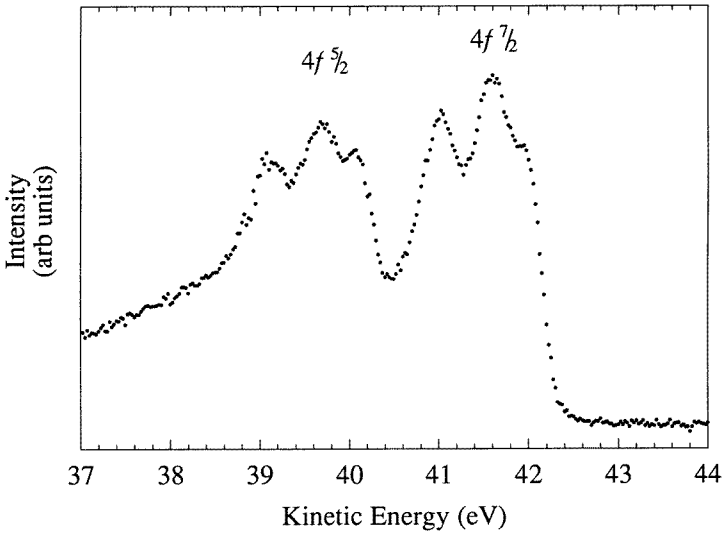

Figure 10. The normalized residuals $Q(E)$ for the Ta 4f levels in $4H_b$-TaS_2 (*a*) for the eight-peak fit shown in figure 8 and (*b*) for the eight-peak fit shown in figure 11, where the cut-off position is permitted to vary.

The model used for all the lines was optd= 8 (see paper I), with the subpeak ratio set to zero for all but the emission from the trigonal prismatic layer (peaks 1 and 5). The Gaussian widths were again constrained to be the same, and as in the 1T case, α was constrained to be the same for corresponding peaks of each half of the spectrum (i.e. the same for peaks 1 and 5 etc). The parameters of the subpeak representing plasmon loss in the trigonal prismatic layer (see paper II) were fixed at the values obtained for 2H-TaS_2, and the cut-off positions of $J(E)$ were also fixed at values obtained earlier. Within the 1T emission, the amplitudes were fixed in the ratio 1:6:6, but as in previous analyses, fixing the 8:6 ratio expected of the corresponding peaks of the spin–orbit-split doublet (again peaks 1 and 5 etc) markedly degraded the quality of the fit, and was not implemented. The results are shown with the data in figure 8, and the fit is apparently very good. The residuals, $Q(E)$ (figure 10(*a*)), still show small systematic errors, and ρ is 586 compared to an ideal value of 297 (319 data points minus only 22 free parameters). The line from site a in the 1T layer has a fixed $J(E)$. The 2H peaks have moderate asymmetry ($\alpha = 0.19$), though the shoulder from the subpeak in $J(E)$ adds to the apparent asymmetry. The other 1T lines have very low asymmetry compared with those for pure 1T-TaS_2; one has reached the bottom limit of 0.01, the other has $\alpha = 0.05$. The lifetime (Lorentzian) widths are much as expected; the 2H peaks have a width almost negligible compared with the instrumental broadening, and the 1T layer majority peaks are wider, and relatively more so for the $J = \frac{5}{2}$ peaks (7 and 8).

The fit can be improved by allowing the cut-off in $J(E)$ (in addition to α) to vary

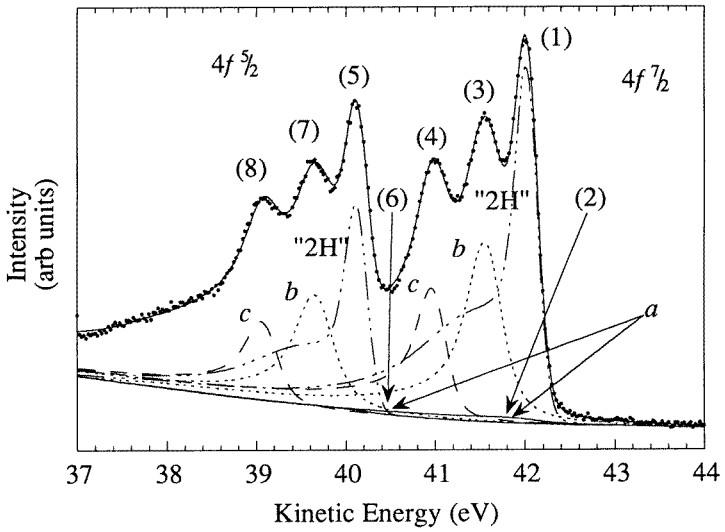

Figure 11. An eight-peak fit to the Ta 4f levels in $4H_b$-TaS_2 with the cut-off position permitted to vary.

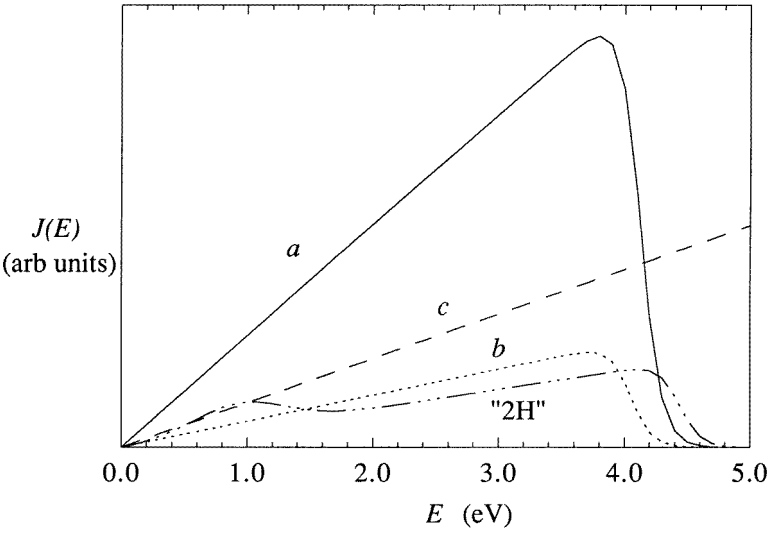

Figure 12. The JDOSs corresponding to the parameters derived from the fits of figure 11.

from the values obtained in paper II for 2H-TaS_2 and in section 2 for 1T-TaS_2. This more realistically models changes in the conduction band structure since, in a rigid-band model, both the initial slope *and* cut-off of the JDOS should change if E_F is shifted by interlayer charge transfer. The result of this less constrained fit is shown in figure 11, and the corresponding residuals in figure 10(*b*). The relevant fitting parameters are summarized in table 1, and the corresponding $J(E)$s are shown in figure 12; the Gaussian width for each peak was 0.268 eV. ρ has dropped to 516, still higher than a statistically acceptable

model, but a significant improvement nonetheless. $J(E)$ for the 2H peaks is hardly affected in shape, though α for these two lines has fallen to 0.13. The cut-off in $J(E)$ for the lowest KE of the 1T peaks (site c) has increased to its upper limit, becoming more DS-like. The spectrum covers a range only 5 eV down from the highest-KE peak, so any cut-off in $J(E)$ above 5 eV will occur off-scale to low KE and is equivalent to modelling with a DS lineshape. With this small modification in the shape of $J(E)$ there is a surprisingly large modification to the overall spectrum and the weight of the emission is shifted more into the 1T layer lines; the asymmetries return to a more familiar 0.17 and 0.30 for emission from sites b and c respectively, though that for site a, the weakest peak present, still appears to be unphysically large.

The problem with this analysis is the variety of models, constraints and bounds available, compared with the quality of the data. For example, it was found that constraining the amplitude ratio of the 2H peaks to be 8:6 was inappropriate, as it was in paper II. But what ratio would be acceptable for the sake of an improved fit? 2:1 might be, but 5:1 would not, and such a fit would by unphysical, even though ρ would be reduced. The Lorentzian widths also present some problems; they are clearly not the same for any of peaks 3, 4, 7 or 8, but should final values such as 1.00, 0.01, 0.30 and 0.40 respectively be accepted? Surely not, as the first two (sites b and c for the $J = \frac{7}{2}$ emission) and the last two (sites b and c for the $J = \frac{5}{2}$ emission) are so inconsistent. Setting the constraints as inequalities does not help. It was increasingly obvious as SHAPER was developed that a final parameter at its upper or lower bound usually reflects an unphysical final result, and the only way to achieve a physically reasonable result with data of this quality is to maintain suitable constraints on parameters. Figures 8 and 11 are the best *physically reasonable* results of scores of attempts to fit the data using a variety of different lineshapes, and represent a balance between real physics and undue empiricism. Table 1 also compares the lineshapes for $4H_b$-TaS_2 with the corresponding peaks in 2H-TaS_2 (paper II) and 1T-TaS_2 (section 2).

3.4. Discussion for $4H_b$-TaS_2

The sextuplet 4f spectrum for $4H_b$-TaS_2 is supporting evidence in itself of interlayer charge transfer, in that the 2H lines occur at higher KE than the mean for the 1T layers, but the details of the lineshapes reveal more about the charge transfer and how it affects the CSW, and table 1 shows some remarkable similarities *and* differences between the lineshapes for the pure polytypes (1T and 2H) and the mixed polytype ($4H_b$).

Consider first the CDW-induced splitting between the lines from sites b and c. The fits improve on the earlier estimates: for $4H_b$-TaS_2, $\Delta E_{CDW} = 0.58 \pm 0.01$ eV; for 1T-TaS_2, $\Delta E_{CDW} = 0.70 \pm 0.01$ eV. The amplitude of the CDW is therefore considerably less in the octahedral layers of $4H_b$-TaS_2 than in pure 1T-TaS_2, but, although this is consistent with charge transfer from the octahedral to the trigonal prismatic layers in $4H_b$-TaS_2, it is not conclusive. Thermodynamic arguments also suggest that the CDW is somewhat weaker in $4H_b$-TaS_2, where the commensurate CDW phase is present up to 315 K [7], whereas in 1T-TaS_2 the CDW, while commensurate only up to 180 K, persists in quasi-commensurate form up to 352 K. From this it is difficult to draw conclusions about the reduction in total energy afforded by the PLD-CDW because of this $1T_3$ to $1T_2$ transition.

For $4H_b$-TaS_2 the difference between the binding energy of the 2H line and the weighted mean of the 1T lines is $\Delta E_{2H-1T} = 0.69 \pm 0.02$ eV, comparable with the CDW splitting for 1T-TaS_2 and suggesting transfer of a significant fraction of an electron per atom from the 1T to the 2H layers. The detailed lineshapes can also reveal something about where the charge has moved.

The Lorentzian (lifetime) widths of the 2H peaks (1 and 5) are small compared with the instrumental Gaussian width, and so are subject to large relative errors, but the site c peaks (4 and 8) for the octahedral layer of $4H_b$ have almost identical lifetime widths to those for 1T itself; the starting values for peaks 4 and 8 were both 0.200 eV, so the convergence on 0.123 eV (peak 4) and 0.181 eV (peak 8), each to within 0.001 eV, is certainly not an artefact of the initial parameter set. The α-values for these lines are similarly well matched. α is constrained to be the same for peaks 4 and 8, and is 0.299 (starting from 0.240) for $4H_b$ and 0.303 for 1T. The cut-off in $J(E)$ is apparently different, at 5 eV for 1T and 9 eV (the upper limit) for $4H_b$, but with these high values any difference will not be apparent in the lineshape at less than 5 eV below the peak, where both lines have a DS shape, and it is therefore irrelevant. The conclusion from this remarkable similarity is that the LDOS at Ta site c in $4H_b$-TaS_2 is almost identical to that for site c in $1T_3$-TaS_2—wherever the charge is transferred from, it is not from site c.

Peaks 3 and 7 (from site b) have Lorentzian widths which are greatly increased in the $4H_b$; the core-level hole is, for whatever reason, shorter lived. Their asymmetry has fallen from 0.236 to 0.175 and the cut-off position in $J(E)$ has moved from 4.0 eV to 2.6 eV, indicating a cut-off in the conduction band closer to E_F. Charge depletion in a band with an upsloping DOS could explain such a combination, but the complexity of the three-manifold conduction band in $1T_3$-TaS_2 makes such a simple picture unreliable.

No clear conclusions can be drawn for the minority (site a) peak for 1T-TaS_2 and the octahedral layer of $4H_b$-TaS_2; to obtain a meaningful fit, it was necessary to assume that the lineshape was unchanged for $4H_b$, but any errors in its small amplitude are likely to have only second-order effects on the overall fit. Peaks 1 and 5 from the trigonal prismatic layer were treated differently for the 2H-TaS_2 and $4H_b$-TaS_2 fits; for $4H_b$ the α-values were constrained to be the same for both peaks (as was the case for the six 1T lines) while for 2H they were not. This has little effect as the α values for 2H-TaS_2 were similar (0.139, 0.146). Compare this with 0.130 for both lines in $4H_b$-TaS_2. The fits are generally insensitive to the cut-off position, and the difference there (3.9 eV for 2H, 4.4 eV for the trigonal prismatic layers in $4H_b$) is not significant. The difference in α is more significant: the 2H peaks are the most intense, and, being at the highest KE, peak 1 is least affected by the lower-KE tails of the other lines. The difference is not great, but implies that the LDOS at E_F in the trigonal prismatic layers in $4H_b$-TaS_2 is lower than in 2H-TaS_2, as for the transition metal intercalates of 2H-TaS_2, where charge transfer into the conduction band also reduced the asymmetries (paper II); here again, an increase in occupancy of the sharply peaked d_{z^2} band *decreases* the DOS at E_F.

Taken altogether the evidence points to the following conclusion. The amplitude of the CDW in $4H_b$-TaS_2 is lower than in 1T-TaS_2, and there is charge transfer from the 1T layers into the trigonal prismatic layers in $4H_b$-TaS_2. The LDOS at site c is very similar in both polytypes, but at site b the LDOS is quite different in the two polytypes. It seems therefore that the bulk of the charge transferred from the 1T layers must come from site b rather than site c.

4. Conclusion

The fitting procedures used for the Ta 4f lineshapes indicate that different asymmetries can be observed for XPS lines originating from neighbouring Ta atoms in 1T-TaS_2 and the octahedral layers. These, and the chemical shift between emission from the trigonal prismatic and octahedral layers in $4H_b$-TaS_2, can be related to the LDOSs at particular Ta sites. For $4H_b$-TaS_2, the site-specific properties of the core-level lineshapes and binding

energies confirm that charge transfer occurs from the octahedral to trigonal prismatic layers, and also suggest that the transfer comes from Ta site b (and perhaps also from site a) in the CDW-modulated layer (where the charge density is higher to start with), rather than from site c. Photoemission from the conduction band would be unable to distinguish the Ta sites in this way. As a complementary technique, only STM could assist in determining the local properties.

Acknowledgments

This work was supported by the UK Engineering and Physical Science Research Council. The authors also gratefully acknowledge the assistance of the staff of the Synchrotron Radiation Facility at the EPSRC Daresbury Laboratory, particularly Dr F Quinn and Dr D Law.

References

[1] Hughes H P and Scarfe J A 1996 *J. Phys.: Condens. Matter* 1439–55
[2] Hughes H P and Scarfe J A 1995 *Phys. Rev. Lett.* **74** 3069
[3] Wertheim G K, diSalvo F J and Chiang S 1976 *Phys. Rev.* B **13** 5476
[4] Hughes H P and Pollak R A 1976 *Commun. Phys.* **1** 61
[5] Hughes H P and Scarfe J A 1996 *J. Phys.: Condens. Matter* 1421–38
[6] Wilson J A, diSalvo F J and Mahajan S 1974 *Phys. Rev. Lett.* **32** 882
[7] Wilson J A, diSalvo F J and Mahajan S 1975 *Adv. Phys.* **24** 117
[8] Wilson J A 1990 *J. Phys.: Condens. Matter* **2** 1683
[9] Claessen R, Burandt B, Cartensen H and Skibowski M 1990 *Phys. Rev.* B **41** 8270
[10] Wertheim G K, diSalvo F J and Chiang S 1976 *Phys. Rev.* B **13** 5476
[11] Hughes H P and Pollak R A 1976 *Phil. Mag.* **34** 1025
[12] Smith N V, Kevan S D and diSalvo F J 1985 *J. Phys. C: Solid State Phys.* **18** 3175
[13] Pollak R A, Eastman D E, Himpsel F J, Heimann P and Reihl B 1981 *Phys. Rev.* B **24** 7435
[14] Coleman R V, Giambattista B, Hansma P K, Johnson A, McNairy W W and Slough C G 1988 *Adv. Phys.* **37** 559
[15] Manzke R, Anderson O and Skibowski M 1988 *J. Phys. C: Solid State Phys.* **21** 2399
[16] Mattheiss L F 1973 *Phys. Rev.* B **8** 3719
[17] Thomson R E, Walter U, Ganz E, Clarke J, Zettl A, Rauch P and diSalvo F J 1988 *Phys. Rev.* B **38** 10 734
[18] Slough C G, McNairy W W, Coleman R V, Garnaes J, Prater C B and Hansma P K 1990 *Phys. Rev.* B **42** 9255
[19] Remskar M, Prodan A and Marinkovic V 1993 *Surf. Sci.* **287–8** 409
[20] Coleman R V, McNairy W W and Slough C G 1992 *Phys. Rev.* B **45** 1428
[21] Giambattista B, Slough C G, McNairy W W and Coleman R V 1990 *Phys. Rev.* B **41** 10 082
[22] Hasegawa T, Yamaguchi W, Kin J-J, Wei W, Nantoh M, Ikuta H, Kitazawa K, Manivannan A, Fujishima A and Uchinokura K 1994 *Surf. Sci.* **314** 269
[23] Kim J-J, Yamaguchi W, Hasegawa T and Kitazawa K 1994 *Phys. Rev. Lett.* **73** 2103
[24] Beal A R 1978 *J. Phys. C: Solid State Phys.* **11** 4583
[25] Tatlock G J 1976 *Commun. Phys.* **1** 87
[26] Friend R H 1979 *PhD Thesis* University of Cambridge